SHOCK INDUCED VAPORIZATION OF SILICA: IMPLICATIONS FOR GIANT IMPACT EVENTS. R.G. Kraus[1], S.T. Stewart[1], D.C. Swift[2], C.A. Bolme[3], R. Smith[2], S. Hamel[2], B. Hammel[2], D.K. Spaulding[4], D.G. Hicks[2], J.H. Eggert[2], and G.W. Collins[2], [1]Harvard University, Dept. Earth & Planetary Sci., Cambridge, MA 02138 (rkraus@fas.harvard.edu), [2]Lawrence Livermore National Laboratory, Livermore, CA 94559, [3]Los Alamos National Laboratory, Los Alamos, NM 87545, [4]U.C. Berkeley, Dept. Earth & Planetary Sci., Berkeley, CA 94720.

Introduction: Giant impacts melt and vaporize a significant amount of the colliding bodies. The degree of vaporization during giant impacts is important to a number of problems in the planetary sciences. For example, the vapor produced during the lunar-forming impact affects the dynamics of the proto-lunar disk [1] and aids in equilibration of oxygen isotopes between the bolide and proto-earth [2]. During the end stages of planetary accretion, the impact vapor plume erodes the pre-existing atmosphere [3]. In extrasolar systems, recent giant impact events are inferred from the presence of amorphous dust and silica gas [4, 5].

Predicting the relative amounts of melt and vapor produced during an impact requires knowledge of the liquid-vapor phase boundary and thermodynamic properties of geologic materials over a tremendous range of pressure-temperature space. The necessary data are lacking due to the experimental difficulties of studying materials near their critical points using static techniques. Even our knowledge of the liquid-vapor phase boundary for one of the most important and well studied minerals, SiO_2, is rather limited [6].

We investigate the liquid-vapor coexistence region of silica by shocking α-quartz to a supercritical fluid state and allowing it to isentropically expand to a state on the liquid-vapor phase boundary. Although planar shock compression and release has been used to study vaporization of a few metals [7-9], this method has only recently been applied to geologic materials [10].

Experimental Method: The Janus laser of the Jupiter Laser Facility at Lawrence Livermore National Laboratory was used to drive 120 to 330 GPa supported and planar shock waves through ~100 μm thick single crystal α-quartz targets. The pressure history in the sample was determined using the known Hugoniot [11] and measured shock velocity, using a line-imaging velocity interferometer system for any reflector (VISAR). The sample decompressed upon shock wave arrival at the downrange free surface where two complementary diagnostic techniques probed the liquid-vapor phase boundary of SiO_2.

Post-shock density measurements. The density of the expanding liquid-vapor mixture was constrained by allowing the decompressing silica to expand uniaxially across gaps of known dimension and stagnate against a LiF window. From the measured silica expansion velocity and particle velocity in the window, the average density of the decompressed state was determined from conservation of momentum.

Shock and Post-Shock Temperature Measurements. Time-resolved thermal emission from the shock front and decompressed state was measured using a line-imaging streaked optical pyrometer [12]. The pyrometer was calibrated to ~10% accuracy using the known shock temperature and reflectivity of α-quartz as a function of shock wave velocity [13], assuming gray-body emission.

Interpretation of Post-Shock Emission: From first principles molecular dynamics simulations based on density functional theory, we calculated the opacity of silica liquid and vapor in the visible spectrum. The silica liquid in the 4000–6000 K temperature range is opaque with an optical depth of a few hundred nm, and the vapor is transparent with an optical depth of at least 100 μm. Consequently, on the time scale of a few ns, thermal emission from the decompressed and boiling liquid originates from the interface between liquid and vapor. Assuming decompression is an equilibrium process, the interface between liquid and vapor is on the liquid-vapor phase boundary. Decompression of the entire sample across the phase boundary requires a finite amount of time, allowing for direct observations of the boundary state. The first experiment to interpret post-shock temperatures in this manner was that for H_2O ice shocked to supercritical fluid and then released to the liquid-vapor boundary [14].

Results: Under the commonly-used assumption of gray-body emission and a measured negligible reflectivity at the wavelength of the VISAR probe laser (527 nm), we determined the temperature of silica on the liquid-vapor phase boundary. Figure 1 presents the shock and post-shock temperatures of silica in a simplified temperature-pressure phase diagram. The pressure corresponding to each observed post-shock temperature is assumed to be on the theoretical liquid-vapor phase boundary from the M-ANEOS model for SiO_2 [6], hereafter referred to as M07. The inferred density of the expanded state (about 0.3 to 0.9 g cm^{-3}) is in good agreement with the model.

However, the temperature-pressure phase diagram does not present the maximum amount of information gleaned from the experiments. A temperature-entropy phase diagram is optimal for examining adiabatic and isentropic processes, such as release from the shocked state.

In Figure 2, we present the shock and post-shock temperatures as a function of entropy. We calculated the entropy along the fluid region of the quartz Hugoniot via two different thermodynamic paths. Our entropy calculation relies on measured thermodynamic parameters for α-quartz [15], stishovite [16, 17], silica liquid [18], and supercritical fluid [11, 13, 19].

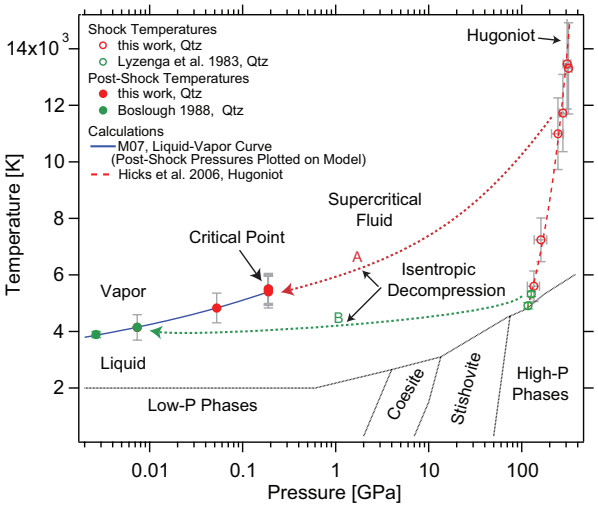

Figure 1: Temperature-pressure phase diagram of silica. In each experiment, quartz is shocked to a fluid state on the Hugoniot (open symbols) and then decompresses isentropically to the liquid-vapor curve (filled symbols) along schematic paths A and B, starting at ~310 and ~120 GPa.

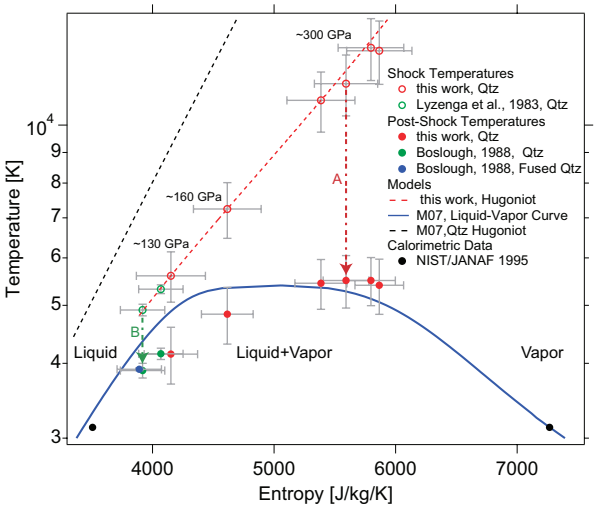

Figure 2: Data from Fig. 1 on a temperature-entropy phase diagram for silica. The shock wave rapidly compresses the silica, increasing the entropy. Because decompression is isentropic, paths A and B are vertical lines.

Discussion: The distinct plateau in the post-shock temperature with increasing entropy, seen in Figure 2, indicates the temperature at the critical point. Hence, the M07 liquid-vapor curve predicted in [6] provides an accurate thermodynamic description of silica near the liquid-vapor coexistence region.

Note, however, that the entropy along our calculated Hugoniot is much higher than that of the M07 model Hugoniot. One source of the disparity is due to a heat capacity greater than the Dulong-Petit limit in the silica supercritical fluid [13]. The physical origin of the high heat capacities is still under debate; however, the implications are immediately recognizable and quantifiable: the entropy of vaporization is reached at lower shock pressures. Our new data and the M07 model predict critical shock pressures of ~100 GPa for incipient vaporization upon release to 1 bar. However, our critical shock pressure for complete vaporization is only 665 GPa, compared to 1650 GPa in the M07 model. Consequently, much more quartz is vaporized during a giant impact event than previously thought.

Conclusions: This work represents a major advancement in our understanding of shock-induced vaporization of silica. We have demonstrated the advantages of shock and release experiments for investigating the experimentally elusive liquid-vapor phase boundary. The data presented are the first to constrain the equation of state of silica up to the critical point on the liquid-vapor phase boundary. By calculating the entropy along the Hugoniot, we revise the amount of silica vapor produced during planetary collisions. Greater vapor production has significant consequences for the moon-forming impact and atmospheric blowoff from giant impacts.

Acknowledgements. This work was funded by LLNL LDRD "Exploring Giant Planets" and DOE NNSA SSGF program (DE-FC52-08NA28752). We thank the techanical staff of JLF, Walt Unites, and Stephanie Uhlich.

References: [1] Stevenson, D.J. (1987) *Annu. Rev. Earth Pl. Sc.* **15**, 271-315. [2] Pahlevan, K. and D.J. Stevenson (2007) *EPSL* **262**(3), 438-449. [3] Ahrens, T.J. (1993) *Annu. Rev. Earth Pl. Sc.* **21**, 525-555. [4] Lisse, C.M., et al. (2009) *ApJ.* **701**(2), 2019-2032. [5] Weinberger, A.J., et al. (2011) *ApJ.* **726**(2), 76. [6] Melosh, H.J. (2007) *MAPS* **42**(12), 2079-2098. [7] Brannon, R.M. and L.C. Chhabildas (1995) *Int. J. Impact Engng.* **17**, 109-120. [8] Pyalling, A., et al. (1998) *Int. J. Thermophys.* **19**(3), 993-1001. [9] Ternovoi, V.Y., et al. (1998) *SCCM-1997*, AIP: Woodbury, New York, p. 87-90. [10] Kurosawa, K., et al. (2010) *GRL* **37**(23), L23203. [11] Knudson, M.D. and M.P. Desjarlais (2009) *PRL* **103**(22), 225501. [12] Spaulding, D.K., et al. (2007) *SCCM-2007*, AIP: Melville, NY, p. 1071-1074. [13] Hicks, D.G., et al. (2006) *PRL* **97**(2), 025502. [14] Stewart, S.T., A. Seifter, and A.W. Obst (2008) *GRL* **35**(23), L23203. [15] Fei, Y.W. and S.K. Saxena (1986) *Phys. Chem. Miner.* **13**(5), 311-324. [16] Luo, S.N., et al. (2002) *GRL* **29**(14), L015627. [17] Akins, J.A. and T.J. Ahrens (2002) *GRL* **29**(10), L014806. [18] Eriksson, G. and A.D. Pelton (1993) *Metall Trans B* **24**(5), 807-816. [19] Lyzenga, G.A., T.J. Ahrens, and A.C. Mitchell (1983) *JGR* **88**(NB3), 2431-2444.